

Article

Precisely Assembled Nanofiber Arrays as a Platform to Engineer Aligned Cell Sheets for Biofabrication

Vince Beachley ^{1,2}, R. Glenn Hepfer ¹, Eleni Katsanevakis ¹, Ning Zhang ^{3,*} and Xuejun Wen ^{3,4,*}

¹ Clemson-MUSC Bioengineering Program, Department of Bioengineering, Clemson University, Charleston, SC 29425, USA

² Department of Biomedical Engineering, Rowan University, Glassboro, NJ 08028, USA

³ Institute for Engineering and Medicine, Virginia Commonwealth University, Richmond, VA 23284, USA

⁴ Institute for Biomedical Engineering and Nano Science, Tongji University School of Medicine, Tongji University, Shanghai 200092, China

* Authors to whom correspondence should be addressed; E-Mails: nzhang2@vcu.edu (N.Z.); xwen@vcu.edu (X.W.); Tel.: +1-804-828-5353 (X.W.); Fax: +1-804-828-3846 (X.W.).

Received: 7 May 2014; in revised form: 9 July 2014 / Accepted: 16 July 2014 /

Published: 7 August 2014

Abstract: A hybrid cell sheet engineering approach was developed using ultra-thin nanofiber arrays to host the formation of composite nanofiber/cell sheets. It was found that confluent aligned cell sheets could grow on uniaxially-aligned and crisscrossed nanofiber arrays with extremely low fiber densities. The porosity of the nanofiber sheets was sufficient to allow aligned linear myotube formation from differentiated myoblasts on both sides of the nanofiber sheets, in spite of single-side cell seeding. The nanofiber content of the composite cell sheets is minimized to reduce the hindrance to cell migration, cell-cell contacts, mass transport, as well as the foreign body response or inflammatory response associated with the biomaterial. Even at extremely low densities, the nanofiber component significantly enhanced the stability and mechanical properties of the composite cell sheets. In addition, the aligned nanofiber arrays imparted excellent handling properties to the composite cell sheets, which allowed easy processing into more complex, thick 3D structures of higher hierarchy. Aligned nanofiber array-based composite cell sheet engineering combines several advantages of material-free cell sheet engineering and polymer scaffold-based cell sheet engineering; and it represents a new direction in aligned cell sheet engineering for a multitude of tissue engineering applications.

Keywords: cell sheets; biofabrication; nanofiber; contact guidance; 3D tissue; skeletal muscle regeneration

1. Introduction

Cell sheets have been extensively used in many areas of tissue engineering as the building units for the construction of 3D, complex, multi-cellular tissues using layer-by-layer stacking methods [1–4] or the transplantable elementary structures that fit into tissue defect sites *in vivo* for tissue repair and functional restoration [5–7]. Conventional approaches to fabricate cell sheets involve cell culture on a substrate and waiting for cell confluence to form a sheet before harvesting for the next steps of the application. There are many problems associated with these approaches, including that the waiting time necessary for the cells to reach confluence may be long, the cell sheets are too fragile to allow handling and damage to critical cell surface proteins, as well as cell-cell junctions of the cell sheets when the proteolytic digestion method is used [8,9]. Recently, minimally-invasive methods have been developed to harvest intact cell sheets using thermo-responsive polymers as culture substrates [4,10,11]. These polymers possess low critical solution temperatures (LCST), below which the polymers are hydrophilic and soluble in water, but above which the polymers are hydrophobic and insoluble [12–15]. By lowering the temperature, confluent cells cultured on the thermo-responsive polymers may be spontaneously detached and recovered as a contiguous cell sheet without the use of conventional proteolytic enzymes. However, even with this method, the waiting time is quite long, and the mechanical properties of the cell sheets are too low to allow subsequent handling and transfer to the desired place [16]. Due to surface tension, cell sheets have the tendency to fold and contract upon surface release, which makes it difficult to handle individual sheets and to manipulate them into complex structures. The ranges of the transition temperatures for the thermo-responsive polymers are wide, and the required low temperatures do not support good cell recovery. In addition, despite a few attempts to accelerate the thermo-harvesting process through chemical modifications of the thermo-responsive polymers [17,18], the required detachment times pose a significant barrier for the use of cell sheets to their full potential.

In the search for a new and enhanced method to fabricate cell sheets, our lab has proposed to incorporate a biomaterial component into the cell sheets while they are being formed. A biomaterial component may provide structural and topographic support to the cell sheets, improve their mechanical strengths, allowing easy harvesting and manipulation, and direct cell behavior and alignment within the cell sheets. A minimal biomaterial content of the composite cell sheets would minimize the foreign body response and inflammatory response associated with the biomaterial, as well as the impedance to cell-cell contact and mass transport to and from the cell sheets. Among different types of biomaterial structures for this task, nanofibers have drawn our attention. Nanofibers have been exploited in many tissue engineering scaffolds to guide cell alignment/tissue formation and direct cell proliferation and differentiation [19–21]. Their exceedingly high aspect ratio, large specific surface area and porosity are beneficial for cell attachment and proliferation [22], reinforcing the cell sheets with minimal amount of materials. Previously, we have reported the successful fabrication of large-surface area (tens of cm²),

ultrathin, uniaxially-aligned nanofiber sheets with a highly-controlled fiber orientation and density using an electrospinning apparatus that is coupled with a novel collecting device designed in our lab [23,24]. To build upon these results, we have explored the potential of the ultrathin-aligned nanofiber sheets as novel substrates for cell sheet engineering.

In this study, a C2C12 myoblast cell line was selected as a model proliferative myoblast cell type that is associated with skeletal muscle, a typical aligned tissue. Ultrathin nanofiber sheets of degradable polycaprolactone (PCL) were seeded with C2C12 myoblasts to allow cell sheet formation upon confluence. Alternatively, C2C12 myoblasts were directly loaded to the nanofiber sheet scaffolds while embedded in fibrin gel films. Characterization of the cells within the composite nanofiber/cell sheets indicated high viability, uniaxial alignment in the direction of fiber orientation and active expression of the phenotypic marker skeletal myosin heavy chain during the entire experimental period up to three weeks during *in vitro* culture. Aligned linear myotubes were seen on both sides of the composite cell sheets despite single-side cell seeding. It is estimated that the mechanical strength of the composite cell sheets were increased by 2–3 orders of magnitude due to the contribution of the nanofiber component. The handling properties of the composite cell sheets have allowed easy transfer from the culture dish and further processing into 3D, aligned tissue structures of higher hierarchy by stacking or self-assembly/bundling. Preliminary implantation of the 3D cable-like construct fabricated from the composite cell sheets into the paravertebral muscle in mice indicated excellent cell viability within the construct, the integrity of the gross morphology and internal microstructures of the construct and the nice integration of the construct with the surrounding tissues. Long-term implantation studies are underway to assess the potential of the 3D constructs from nanofiber-reinforced cell sheets for many aligned tissue engineering applications.

2. Experimental Section

2.1. Electrospinning

Polycaprolactone (PCL, Mn~80,000, Sigma, St. Louis, MO, USA) was dissolved in dichloromethane and dimethylformamide (3:1) (DCM:DMF, Sigma) at a concentration of 17% wt/v. Polymer solution was fed by syringe pump (Medfusion 2010i; Smiths Medial Inc., Carlsbad, CA, USA) at a rate of 0.025 mL/min through a 21 G blunt-tipped needle. A voltage of 9 KV was applied to the needle tip with a high voltage power supply (ES40P-10W, Gamma High Voltage Research, Ormond Beach, FL, USA). Nanofibers were collected using a custom-built collecting device designed in our lab [23,24]. The device utilizes electrostatic forces to deposit aligned nanofibers across the air gap between two computer-controlled parallel mobile tracks, which continuously distribute and assemble the aligned fiber arrays into sheets with a controllable fiber density. The needle tip was held at 10 cm above this device during electrospinning, while the parallel mobile tracks pulled electrostatically-aligned electrospun fiber arrays into a secondary collection area at a vertical speed of 21 mm/s. Ultra-thin aligned fiber mats were assembled on a rectangular rack simultaneous to fiber collection, and the fiber density was varied, with collection times ranging from 5 to 30 min. Ultra-thin aligned PCL nanofiber sheets were attached to thin 25-mm inner diameter 316L stainless steel rings for *in vitro* cell culture in 6-well plates. Aligned nanofiber mats with variable density were fabricated by varying the collection

time, and crisscrossed nanofiber mats were fabricated by attaching two nanofiber arrays to a steel ring at a 90° angle relative to each other. The mounted nanofiber sheets on the stainless steel rings are referred to as “scaffolds”.

Fiber Density Variation

The fiber density of thin aligned nanofiber sheets was defined as the number of nanofibers crossing a line that is perpendicular to the direction of fiber alignment. Fiber density was measured based upon scanning electron microscope (SEM) images. The fiber density of ultra-thin aligned nanofiber sheets was proportional to the electrospinning collection times. Aligned nanofiber arrays with densities ranging from 0.1 to 1.1 fibers/ μm were fabricated to determine the effects of fiber density on cell confluence and alignment in composite nanofiber/cell sheets. C2C12 cells were seeded and cultured as described in Section 2.2 for 1, 3 or 7 days. Actin filaments and nuclei were stained, and cell alignment and the percent cell confluence were calculated based upon measurements on fluorescent images. Cell alignment was defined as the angular deviation of the long axis of a cellular actin filament. Ten randomly selected cells were used for cell alignment measurements within a single image. The percent of cell confluence was defined as the % of the total area occupied by actin-stained cell bodies. The total unstained area in images was calculated and subtracted from the overall area to obtain a value for the % of area occupied by cells. For both cell alignment and the percent of cell confluence calculations, three independent samples were used for each group, and 2 images were taken at random locations on each sample for analysis.

2.2. Composite Nanofiber/Cell Sheets

C2C12 myoblasts were either directly seeded on the nanofiber scaffolds or loaded to the nanofiber scaffolds with fibrin gel. Nanofibers were suspended across a metal ring to form a circular scaffold area with a 25-mm diameter for cell seeding. The scaffolds contained a single layer of aligned nanofibers at a density of 0.1–1.1 fibers/ μm . The average diameter of the electrospun nanofibers was ~700 nm, so the thickness of the scaffolds prior to seeding can be estimated to be ~700 nm. For direct cell seeding, C2C12 myoblasts were cultured in T-75 flasks to 80% confluence in DMEM media with 10% fetal bovine serum (FBS). Aligned nanofiber scaffolds were sterilized in 75% ethanol for 30 min, washed with PBS and then immersed in media. Cells were trypsinized and resuspended in media at approximately 1 million cells per mL. Half of a milliliter of the cell suspension was dripped evenly over each scaffold. Scaffolds were incubated in DMEM media supplemented with FBS for 5 days. Media was changed every 48 h. When myotube differentiation was desired, media was changed to DMEM media with 10% horse serum after 5 days.

For direct cell loading with fibrin gel, bovine fibrinogen (MP Biomedicals, Santa Ana, CA, USA) was dissolved in 1×PBS at a concentration of 15 mg/mL and vacuum-filtered with 0.45 μm filters for sterilization. Bovine thrombin (MP Biomedicals) was dissolved in DMEM culture media at a concentration of 100 U/mL and sterile filtered with 0.45- μm filters. C2C12 myoblasts were suspended in fibrinogen or thrombin solutions at a concentration of 500,000 cells/mL. Nanofiber scaffolds were immersed in fibrinogen and thrombin cell suspensions, respectively. Removal from the suspensions resulted in the formation of thin fibrinogen or thrombin liquid films containing suspended cells on the

nanofiber scaffolds [25]. The cell-containing fibrinogen and thrombin thin films were then sandwiched together and in close contact. Polymerization of fibrinogen and thrombin produced a fibrin gel film with entrapped myoblasts on the surfaces of the nanofiber scaffolds. The thickness of fibrin gels after crosslinking was estimated from cryosections to be approximately 20 μm (data not shown). The cell-containing constructs were incubated for 1–7 days.

2.3. Mechanical Testing

Composite nanofiber/cell sheets with a fiber density of ~ 0.85 fibers/ μm were cultured for 5 days in proliferation media and an additional 3 weeks in differentiation media. Tensile testing was performed on cell sheets using a Shimadzu EZ Graph tensile tester with a 50 N load cell (Nakagyo-ku, Kyoto, Japan) and Trapezium 2.32 software for data acquisition. Samples were removed from an incubator immediately prior to testing and remained covered in media throughout. A square of nanofiber/cell composite sheet was cut to the dimensions of 7 mm \times 7 mm. The ends were attached to the grips of the mechanical testing machine. Samples were strained at a rate of 0.3 mm/s (4.3%/s) until fracture, and the elastic modulus was determined from stress-strain curves. The elastic modulus of nanofiber/cell sheets was measured at the region of maximum slope before the onset of elastic failure. Five samples were tested for each group.

2.4. Multilayered Nanofiber/Cell Sheet Constructs

Multilayered constructs were fabricated by stacking several single-composite cell sheets layer-by-layer to form a thick construct. Composite nanofiber/cell sheets were taken out of media, blotted at their edge to remove excess media and placed on top of one another. Cell sheets were left attached to their supporting rings during stacking to ensure a smooth interface between layers without any folding or wrinkles. The outer support rings of each layer rested on each other, and the direction of fiber alignment was matched up for each layer. The metal rings supporting the cells sheets were physically tied together with 4 loops of suturing at their top, right, left and bottom edge to ensure that the layered cell sheets remained in close contact with one another. Media was intermittently dripped over the multilayered construct for up to two hours to allow for cell adhesions to form between layers before returning the constructs to an aqueous environment. Constructs were cultured up to 5 days.

2.5. Self-Assembled Aligned 3D Cable Structures

To explore the possibility of fast-forming, three-dimensional, aligned cable structures mimicking tissues with aligned structures, such as skeletal muscles, from aligned composite nanofiber/cell sheets, aligned composite cell sheets were first cut parallel to the long axis of the fiber orientation, resulting in an ellipse-shaped hole, due to the contraction of a portion of the sheet into a cable structure along the perimeter of the hole. The sheet underwent further self-assembly into a thicker, rod-like structure when the sheet was cut in the direction perpendicular to fiber/cell alignment at the tips of the hole. These rod-like structures can also be merged to form larger, aligned 3D cable structures.

2.6. Intramuscular Implantation of 3D Cable Structures

3D, aligned cable structures were implanted into the paravertebral muscle on the back of a mouse. Mice were anesthetized with ketamine, and an incision was made along the spine to expose the paravertebral muscle. The cable structures were inserted into the paravertebral muscle. Two ends of the grafts were sutured to the surrounding muscle to anchor the grafts and to provide tension and keep them in place. Mice were sacrificed after 1 day, and the microstructure of the implants was evaluated using histological techniques.

2.7. Histology/Immunohistochemistry

3D cable constructs and cell/nanofiber sheets were fixed in 4% paraformaldehyde for 45 min. Fixed specimens were stained with AlexaFluor 488-conjugated phalloidin (Invitrogen) for actin filament, 4'-6-diamidino-2-phenylindole (DAPI, Invitrogen) for cell nuclei and immunostained with anti-skeletal myosin heavy chain antibody (Sigma) for differentiated myotubes. Selected fibrin gel films were incubated in 2.5% glutaraldehyde overnight and imaged from the autofluorescent signal to visualize the fibrin filaments. The 3D cable constructs were embedded in optimum cutting temperature (OCT) compound, cryosectioned and stained using hematoxylin and eosin (H&E).

2.8. Microscopy/Image Processing

Fluorescent microscope images were taken using a Nikon Eclipse TE2000-S microscope with an EXFO X-cite 120 fluorescence illumination system and a Q-Imaging Micropublisher 3.3 RTV camera. Confocal images were taken with a Leica confocal microscope (TCS SP5 AOBS). Scanning electron microscope (SEM) images were taken at 1,000- to 6,000-times magnification using a Hitachi TM-1000 SEM. An ImagePro Plus (Media Cybernetics, Rockville, MD, USA) was used to analyze SEM images of nanofibers and florescent images of cells to measure fiber diameter, alignment and density and cellular alignment and cell density. Amira software (Visage Imaging, San Diego, CA, USA) was used to reconstruct 3D images from confocal microscopy. Alignment in histological images was quantified using the FibrilTool plug-in applied to the blue channel in ImageJ software [26].

2.9. Statistical Analysis

The Kruskal–Wallis test was used as an initial test for differences within a sample set. For sample sets with a Kruskal–Wallis p -value (p) < 0.05, the Mann–Whitney test was used to evaluate differences between groups. All statistical analysis was done using SPSS software.

3. Results and Discussion

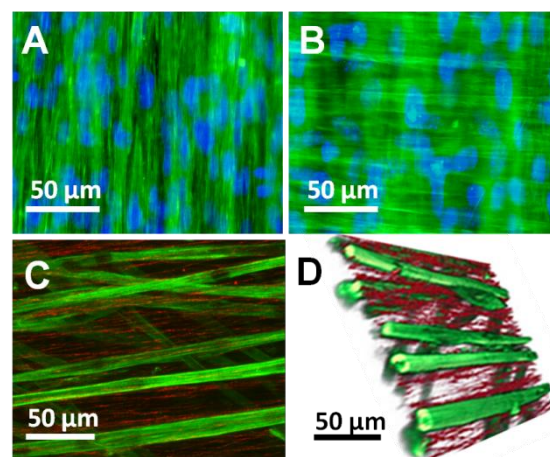
3.1. Electrospinning

PCL nanofiber substrates were made up of free, suspended, aligned fiber arrays with an average fiber diameter of around 700 nm ($\sigma = 80$ nm). The angular deviation of aligned nanofiber arrays was 4° ($\sigma = 0.5^\circ$), and the degree of fiber alignment was not affected by the fiber density.

3.2. Composite Nanofiber/Cell Sheets

C2C12 myoblasts were seeded on nanofiber substrates by dripping cell suspension over them. Cells on aligned nanofibers formed a uniaxially-aligned confluent monolayer (Figure 1A), and cells cultured on crisscrossed nanofiber arrays (Figure 1B) aligned on either layer of nanofibers, forming a confluent monolayer with a crisscrossed pattern, similar to the fiber orientation. Composite nanofiber/cell sheets remained freely suspended on their supporting rings and did not require any procedures for removal from the tissue culture plate surface, as is associated with material-free cell sheets. Images of immunostained composite nanofiber/cell sheets with anti-skeletal myosin heavy chain antibody at three weeks in culture clearly show the presence of differentiated, aligned myotubes on both sides of the nanofiber sheet, despite single-side seeding (Figure 1C,D). This suggests that the level of porosity and the pore size of the nanofiber sheets are sufficient to allow cell migration and molecular exchange across the nanofiber sheets. As a reference, it is estimated that an aligned nanofiber sheet with a fiber density of 0.35 fibers/ μm has a porosity greater than 75% (as calculated by multiplying fiber diameter ($\mu\text{m}/\text{fiber}$) by fiber density (fibers/ μm) and subtracting this value from one). The presence of the nanofiber sheets did not hinder cell differentiation into myotubes on both sides of the sheets. The myotubes appeared to be linear and unbranched and were aligned in the direction of fiber orientation. Our results indicate that the aligned nanofiber sheets have guided the differentiation of myoblasts into aligned, linear myotubes, a highly desirable outcome for *in vitro* skeletal muscle tissue engineering [27].

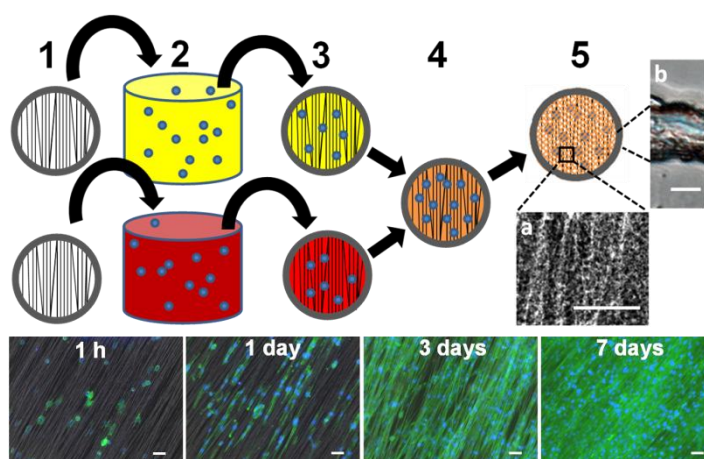
Figure 1. Fluorescent microscope images of C2C12 cell sheets grown on (A) uniaxially-aligned and (B) crisscrossed ultrathin nanofiber substrates for one week. Actin filaments were stained in green; nuclei were stained in blue. Confocal microscope images of a composite aligned nanofiber/cell sheet cultured for three weeks is shown in 2D (C) and reconstructed in 3D (D). Nanofibers (with a fiber density of 0.85 fiber/ μm) are visualized in red, and myotubes are immunostained in green with skeletal myosin heavy chain. Thick multinucleated myotubes are present on both sides of the nanofiber sheet (D), despite single-side seeding.



In parallel groups, C2C12 cells were directly loaded to the nanofiber sheets with fibrin gel (Figure 2). Cells were mixed in fibrinogen and thrombin solutions, respectively. Immersion of nanofiber scaffolds in each solution and their subsequent removal from the solutions resulted in the formation of thin fibrinogen or thrombin liquid films containing suspended cells on the nanofiber sheets. The cell-containing

fibrinogen and thrombin thin sheets were then sandwiched together and in close contact. Polymerization of fibrinogen and thrombin produced a fibrin gel with entrapped myoblasts on the nanofiber sheets. A matrix of fibrin filaments appeared to cover the PCL nanofibers and fill into the spaces in between fibers (Figure 2). The gel films facilitated the attachment of the cells to the nanofiber sheets and the formation of composite nanofiber/cell sheets. Fluorescent images of cell morphology in the composite nanofiber/cell sheets at various time points are shown in Figure 2. Cells were observed embedded in the gel films throughout the composite sheets in a uniform distribution and began to align in the direction of the nanofiber arrays after only one hour of incubation. After one day, cells were aligned and elongated along the fiber long axis. Cell proliferation resulted in confluent aligned composite nanofiber/cell sheets by Day 7.

Figure 2. (Top) One step direct cell seeding with fibrin gel. (1) Mounted nanofiber arrays are immersed in (2) fibrinogen (represented in yellow color) and thrombin (represented in red color) solutions containing suspended cells (represented in blue color), respectively. (3) Removal from the liquid results in the formation of a thin, uniform liquid film over the nanofiber arrays. (4) Fibrinogen and thrombin cell-containing films are sandwiched together and in close contact. (5) A polymerization reaction results in crosslinked fibrin film with embedded nanofibers and cells. **(a)** A close up image of fibrin filaments surrounding the aligned polycaprolactone (PCL) fibers (scale bar = 50 μm). **(b)** a cross-section of a composite fibrin gel nanofiber composite film (scale bar = 10 μm). **(Bottom)** Fluorescent images of nanofiber/cell sheets with direct C2C12 cell fibrin seeding taken at 1 h and 1, 3 and 7 days after fabrication. Actin filaments were stained in green, and cell nuclei were stained in blue. Scale bar = 50 μm .

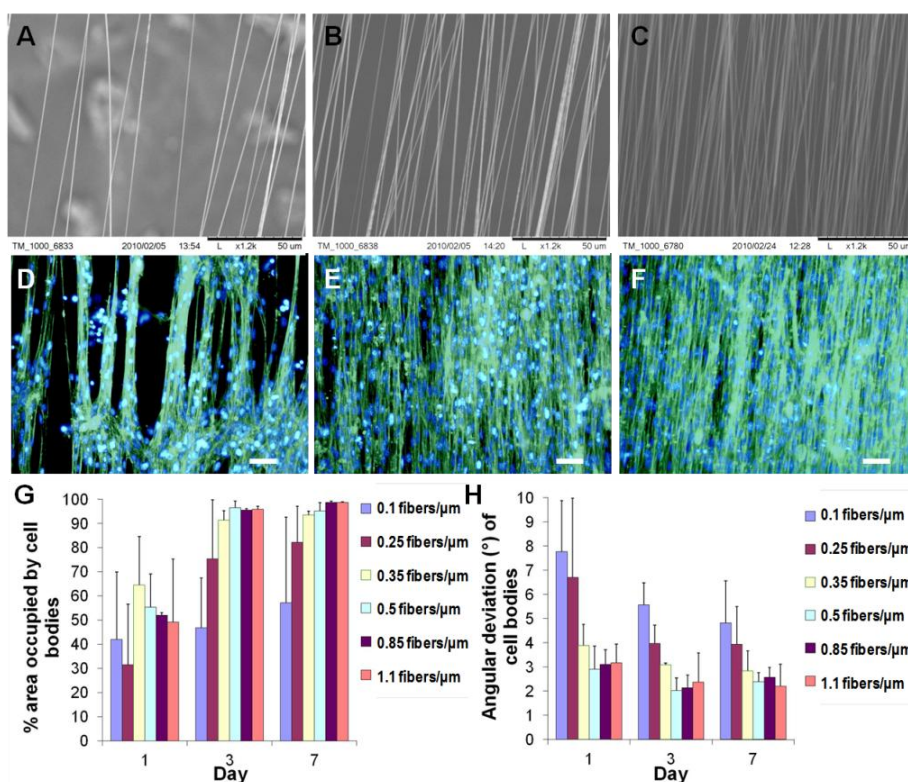


3.3. Fiber Density Variation

To examine the effect of fiber density on cell alignment and the percent of cell confluence pertaining to cell sheet formation, aligned nanofiber arrays with varying fiber densities were fabricated. C2C12 cells were seeded on arrays with aligned fiber densities of 0.1, 0.25, 0.35, 0.5, 0.85 and 1.1 ($\sigma = 0.06, 0.07, 0.02, 0.07, 0.05, 0.05$) fibers per μm length (measured in the direction perpendicular to fiber alignment) and fixed at 1, 3, and 7 days. Two parameters were evaluated quantitatively. The percent of cell confluence was evaluated as the % of the total area occupied by

actin-stained cell bodies. Cell alignment was evaluated as the angular deviation of the long axis of cellular actin filament from the long axis of nanofiber arrays. Representative images and graphs of percent confluence and cell alignment for all groups are shown in Figure 3. It was found that cells aligned well in the direction of fiber orientation. The standard deviation of the direction of cell elongation from the fiber long axis was between 2–8° for various fiber densities and time points in culture. Statistically significant differences in cell alignment for different fiber densities were not present, but there was an exhibited tendency of increases in cell alignment as fiber density increased. With prolonged time in culture, this tendency became less pronounced (Figure 3H). At three days in culture, a step increase in the percent of cell confluence was seen when the fiber densities exceeded 0.25 fibers/μm. This correlates with the increases in cell alignment at the same time point for the same set of fiber density groups (≥0.25 fibers/μm). It appears that a critical fiber density exists around 0.25 fibers/μm, beyond which both cell alignment and the percent of confluence are greatly promoted. At Days 3 and 7, the percent of cell confluence was above 90% for all groups of fiber densities 0.35 fibers/μm or greater. At Day 7, statistically significant differences ($p < 0.05$) in the percent of cell confluence were present for the 1.1 fibers/μm group *versus* all groups, except for the 0.85 fibers/μm group ($p = 0.827$).

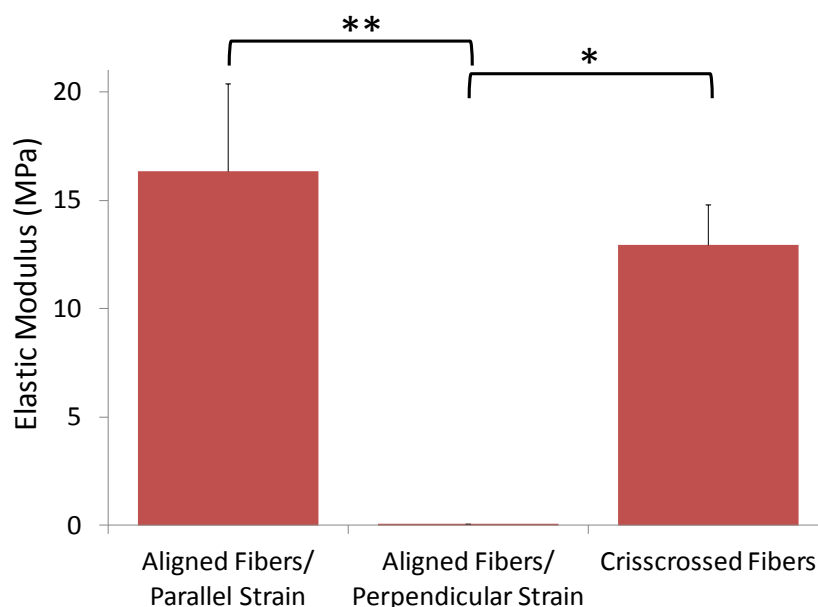
Figure 3. (Top) Representative SEM images of aligned PCL nanofiber sheets of three different fiber densities of (A) 0.1 fibers/μm, (B) 0.35 fibers/μm, and (C) 0.85 fibers/μm. (Middle) C2C12 cells at seven days in culture on the nanofiber sheets of different fiber densities corresponding to those in the top panel. Actin filaments were stained in green, and cell nuclei were stained in blue. Scale bar = 50 μm. (Bottom) Quantitative measurements of the percent of cell confluence (G) and cell alignment (H) of C2C12 cells cultured on aligned nanofiber sheets of fiber densities in the range of 0.1–1.1 fibers/μm.



3.4. Mechanical Properties

Nanofiber/cell sheets with a uniaxial fiber orientation were strained parallel and perpendicular to fiber orientation, and crisscrossed sheets were strained parallel to one of the two directions of fiber orientation. The elastic modulus (Figure 4) of uniaxially-aligned composite sheets were significantly higher ($p < 0.01$) in the direction of fiber orientation ($E = 16.3$ MPa, $\sigma = 4.1$ MPa) compared to the direction perpendicular to the fiber orientation ($E = 0.0612$ MPa, $\sigma = 0.014$ Mpa), which was on the same order of magnitude as what has been reported for individual skeletal muscle cells ($E \sim 0.025$ MPa) measured using atomic force microscopy (AFM) [28]. The elastic modulus of crisscrossed composite sheets ($E = 12.9$ MPa, $\sigma = 1.9$ MPa) remained the same in both directions of the fiber orientation. Acellular nanofiber scaffolds were tested in all three conditions, and their elastic moduli were not significantly different from those of the composite nanofiber/cell sheets for any fiber orientation or direction of strain (data not shown).

Figure 4. Elastic modulus of composite nanofiber/cell sheets. Constructs with a uniaxial fiber orientation were strained in the directions parallel and perpendicular to the fiber long axis, and constructs with crisscrossed fiber orientation were strained in the direction parallel to one of the two directions of the fiber long axis (* $p < 0.05$, ** $p < 0.01$).

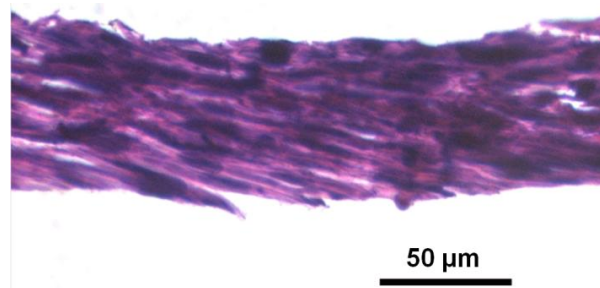


The mechanical data provided strong evidence that the nanofiber component dominated the overall mechanical properties of the composite cell sheets. The contribution of the nanofibers to the mechanical strengths was reflected in the large difference in the elastic modulus parallel and perpendicular to the fiber orientation in uniaxially-aligned constructs. The contribution of the cells to the overall mechanical properties seemed minimal, because the elastic modulus of the composite cell sheets was similar to that of acellular (nanofiber only) control scaffolds for any fiber orientation or direction of strain. In addition, the three orders of magnitude increase in the elastic modulus of the composite sheets in the direction of the nanofiber orientation when compared to that of individual cells was quite significant.

3.5. Multilayered Nanofiber/Cell Sheet Constructs

When two moist nanofiber/cell sheets were placed in physical contact on top of one another in air, they immediately adhered together, due to surface tension. Layer adherence was very smooth without the presence of wrinkles. Multilayered structures were readily assembled through this layer-by-layer procedure, and all of the layers could be assembled at one time. Final, stable assemblies with strong cell-cell adhesion between layers can be developed in 2 h. H&E staining revealed that individual cell sheets adhered intimately within the multilayered structures, appearing to have become homogeneous tissue, and retained uniaxial cell alignment in the direction of the fiber orientation throughout the structure (Figure 5).

Figure 5. Thick, multilayered tissue constructs were formed with aligned nanofiber-cell sheets. The cross-section of a six-layered composite cell sheet construct stained with H&E demonstrates the adhesion among cell layers and cell alignment.

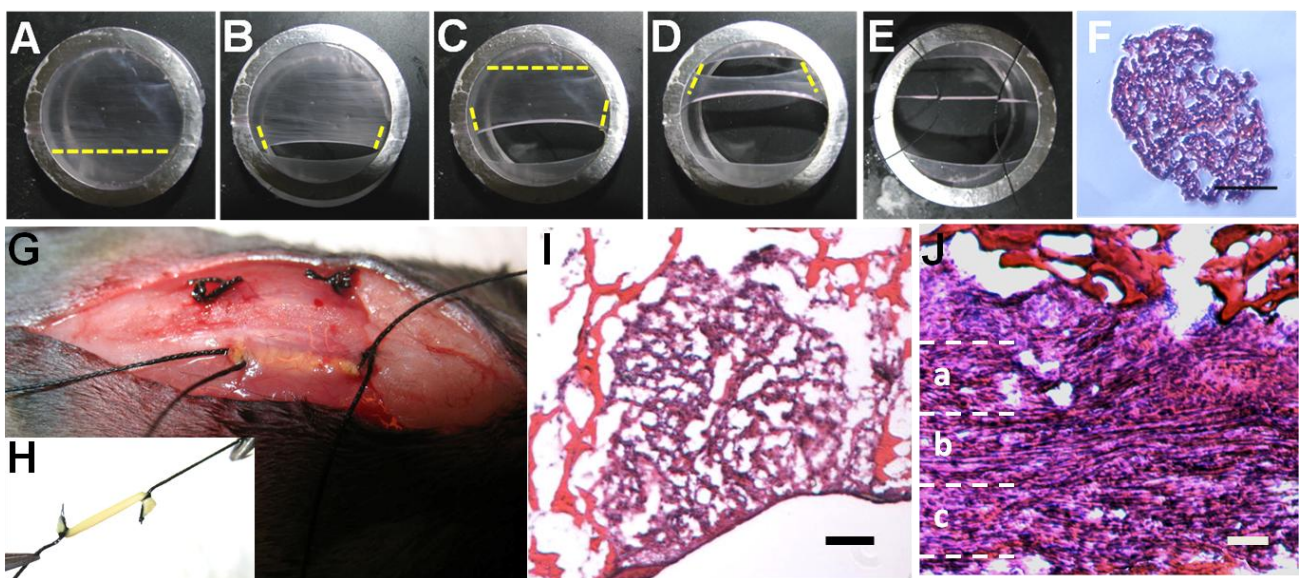


3.6. 3D Aligned Cable Structures

In addition to the stacking of the composite nanofiber/cell sheets to form multilayered constructs, composite cell sheets may be self-assembled/self-rolled into rod-like structures seen in many types of aligned, native tissues, such as skeletal and cardiac muscle, tendon and neural tissues. When the composite cell sheets were cut as shown in Figure 6A–E, they self-assembled/rolled into 3D rod structures, due to fiber and cell tensions within the construct and the surface tension. The cross-section of an aligned (~300 μm diameter) rod structure assembled from a single 25-mm diameter cell/nanofiber sheet is shown in Figure 6F. Several rod-like structures can be further bundled together to form bigger aligned composite nanofiber/cell cable grafts. The cross-section of these cable grafts exhibited a honeycomb-like morphology that may encourage both cell survival within the graft core and vascular and native cell infiltration *in vivo*. Implanted cable grafts in the paravertebral muscle of a mouse also exhibited a honeycomb-like cross-section and retained uniaxial cell alignment after implantation. The gross morphological images of an implant and the surgical procedure are shown in Figure 6H,G, respectively, and cellular arrangement within the graft can be seen in the histological images one day after implantation (Figure 6I,J). The handling properties of the graft allowed easy implantation and securing in place at the tissue site. The graft was robust enough to survive the implantation procedures, while maintaining the integrity of both the gross morphology and the internal microstructures. H&E staining of the retrieved 3D cable graft shows that the graft was densely populated with cells across the entire thickness of the graft and retained cell alignment along the fiber long axis (Figure 6J). Alignment in Figure 6J was quantified at the center and periphery of the graft with ImageJ FibrilTool

plug in. Anisotropy values of 0.24 and 0.34 at the periphery, and 0.42 at the graft center corresponds to high levels of alignment with FibrilTool [26]. There was no core ischemia in the graft, suggesting that the porosity and permeability level of the nanofiber arrays in the graft were sufficient for effective oxygen perfusion and mass transport. At the periphery of the graft, fusion of the graft with the surrounding tissue was seen (Figure 6I,J). The cross-section view of the graft shows that cells attached to the nanofibers well and spread throughout the entire graft (Figure 6I). Both cross-section and longitudinal views of the cable graft evidence skeletal muscle-like structures of a single tissue segment without physical gaps among individual rod-like structures within the graft.

Figure 6. Aligned nanofiber/cell sheets self-assembled into rod-like structures when they were cut in a pattern (A–E). H&E staining of the cross-section of such a structure details its microstructure (F). A thick, aligned nanofiber-cell cable graft (H) was implanted in the intravertebral muscle (G) of a mouse. H&E staining of a retrieved cable graft at one day post-implantation in the cross-section (I) and in the graft long axis (J). Alignment along the graft long axis was quantified using the ImageJ FibrilTool [26] for different regions of the implant. Anisotropy scores were 0.24, 0.42 and 0.34 for regions a, b and c, respectively. Scale bar = 100 μ m.



Cell sheet engineering has vast potential in tissue engineering and has already demonstrated success in *in vivo* applications in the cornea [5], urothelium [29], periodontal ligament [30], blood vessel [31] and cardiac muscle [2]. Advances in micropatterning have increased the versatility of this technology, so that aligned cell sheets can be fabricated to better suit the needs for the regeneration of aligned tissues, such as cornea, blood vessel and muscle [32,33]. This report outlines a novel approach toward cell sheet engineering through incorporating a thin layer of aligned nanofiber sheet. The nanofiber component in the composite cell sheets plays multiple vital functions, including: (1) obviating the need for extended culture time to achieve cell confluence/ECM production prior to handling and cell sheet detachment for harvesting; (2) allowing cell sheet handling/manipulation without disrupting cell-cell contacts or ECM; (3) mechanically strengthening the cell sheets; (4) guiding cell alignment within the sheets; (5) supporting mass transport and molecular exchange between the cell sheets and the local

environment for cell survival and function; and (6) facilitating self-assembly of the cell sheets into 3D tissue structures of a higher hierarchy. None of the other existing methods in cell sheet engineering has achieved all of these functions. We have produced crisscrossed and uniaxially-aligned C2C12 myoblast cell sheets on ultra-thin, extremely low density nanofiber arrays that are fabricated using a novel electrospinning apparatus designed in our lab [23,24]. It was discovered that confluent cell sheets could grow on ultra-thin, low density nanofiber arrays that had extremely high porosity. The porosity of the nanofiber arrays was sufficient to allow aligned linear myotube formation on both sides of the nanofiber arrays in spite of single-side cell seeding. Characterization of the cells within the composite nanofiber/cell sheets indicated high viability, uniaxial alignment in the direction of fiber orientation and robust expression of phenotypic marker skeletal myosin heavy chain during the entire experimental period. The mechanical strength of composite cell sheets was dominated by the nanofiber component, which is estimated to increase the elastic modulus of skeletal muscle cells by 2–3 orders of magnitude in the composite cell sheets. The composite nanofiber/cell sheets can be readily assembled into 3D tissue structures of higher hierarchy by either stacking or self-assembly/bundling. The 3D constructs hold promise as scaffolds for tissue engineering of aligned tissues.

This work represents a shift in the current paradigm in cell sheet engineering, in which bulk biomaterial components are avoided completely to minimize the disturbance to cell-cell contacts and natural ECM production in the cell sheets, and the hampering of the cell sheet-host tissue integration. However, some favorable properties offered by biomaterials are also lost with the material-free approaches for cell sheet engineering. In Table 1, three different approaches for cell sheet engineering, *i.e.*, material-free cell sheets, the composite nanofiber cell sheets presented here and a porous polymer film approach [34], are compared in terms of six properties pertaining to tissue engineering applications. The major advantages of material-free (MF) cell sheets are the absence of any synthetic materials that may cause a foreign body response. In this area, current efforts have been focused on designing novel thermoresponsive (TR) polymers or modifying existing materials to control the range of transition temperature and to shorten the detachment times [18,35]. TR polymer poly(N-isopropylacrylamide) (PIPAAm) was grafted to the surfaces of a culture dish. The reversible adhesion/detachment of the cells to the PIPAAm-grafted surfaces was found to be dependent on the thickness, as well as the nano-topologies of the PIPAAm layer [35]. Further, PIPAAm was chemically modified or grafted to micropatterned cell culture surfaces to modulate site-selective cell adhesion or detachment with temperature control [36,37]. Despite these efforts, fundamental problems with MF cell sheets persist, including extended culture time, poor mechanical and handling properties and limited potential for biomolecule storage/release. For example, MF cell sheets are very fragile and barely survive the manipulations during transplantation or 3D tissue fabrication [38]. Since MF cell sheets contain no material component, natural cell-secreted ECM must be assembled to provide necessary structural support or mechanical properties. This may require long culture times, ranging from two to several weeks [33,39], which are associated with defect formation in the cell sheets and progressive sample loss, due to the fact that cell tensions overcome the adhesion to the culture substrates, leading to premature detachment. Sample loss was reported after 4–6 weeks in culture with loss rates of 30–50% at 10 weeks and accelerated loss afterwards [40]. Another challenge associated with MF cell sheet fabrication is the requirement for sheet detachment. The maintenance of cell-cell junctions during sheet detachment introduces sheet contractility upon surface release that can shrink the surface area of

released cell sheets by up to 90% [41]. Sheet contraction leads to alterations in the sheet morphology that compromise subsequent handling/manipulations.

Table 1. A comparison among three methods in cell sheet engineering, *i.e.*, material-free cell sheets, composite nanofiber/cell sheets and a porous polymer film-based cell sheet in terms of five properties pertaining to tissue engineering applications.

	Structural support for cell sheet	Detachment procedures	Mechanical Properties (elastic modulus: Primary source	Porosity (for cell-cell contacts between layers in multilayer construct)	Synthetic material (associated potential for foreign body response)	Multilayer biofabrication
Material-Free Cell Sheet	•Cell-generated ECM	•Thermal (20–25 °C) [13,18,32] •Mechanical [40]	8.95 MPa: ECM deposited after 10 wk culture with ascorbic acid [40]	100%	None	Gelatin stamp: Cell-cell adhesions Required (~30 min) for addition of each layer [32]
Nanofiber Cell Sheet (0.5–0.85 fibers/μm)	•Electrospun polymer nanofibers •Cell-generated ECM	Not required	10–16 MPa: Polymer nanofibers	40–65%	20–40 μg/cm ²	Simple stacking: cell-cell adhesions for multiple layers were adhered simultaneously
Porous Film Cell Sheet [34] (3–5 μm thickness)	•Solvent cast polymer film •Cell-generated ECM	Not required	20–35 MPa (estimated): Porous polymer film	50%	170–290 μg/cm ²	Not reported

In comparison, the aligned nanofiber substrates have significantly enhanced the mechanical strengths and structural stability of the composite cell sheets. The mechanical strength of the fabricated PCL-C2C12 composite cell sheets, which are dominated by the nanofiber component, is estimated to be orders of magnitude higher than a similar MF C2C12 cell sheet would be. Although mechanical testing data on MF C2C12 cell sheets are not available in the literature, composite C2C12 cell sheets exhibited better mechanical strength than MF cell sheets of other types of cells that were cultured for a longer term to gain mechanical strength. The elastic modulus of our monolayer composite C2C12 sheets in the direction of nanofiber orientation was ~80% higher when compared to multilayer MF sheets of aligned aortic smooth muscle cells, which were cultured for 10 weeks in media supplemented with ascorbic acid to stimulate proliferation and ECM production [40]. A precise comparison between these two cell sheets may not be possible due to the differences in cell types, cell sheet thickness and testing protocols, but their elastic modulus on the same order of magnitude suggests that the nanofiber component of the composite cell sheets is able to fill the mechanical role of supplemented long-term ECM production. Confluent aligned C2C12 cell sheets formed on ultra-thin nanofiber arrays in as few as three days. Thus, the composite nanofiber/cell sheet approach can be used to reduce culture times and sample loss, making cell sheet engineering more compatible with cell types that do not have extensive ECM production. Incorporation of the nanofiber arrays during cell sheet formation also eliminates the need for the detachment step in sheet recovery and maintains the overall shape of the sheets during manipulation.

The handling characteristics of the composite cell sheets are greatly augmented by the nanofiber component. Structural support from the nanofiber component, as well as inherent edge fixation allows the confluent composite nanofiber (CN) sheets to be transferred directly to the host site or assembled into more complex 3D structures as soon as they are confluent. Direct cell loading with fibrin gel enhanced cell attachment to the nanofiber scaffolds for sheet formation without disrupting cell alignment. Because the fibrin matrix (Figure 2a) appeared to be randomly aligned with a porosity much smaller than the size of a cell, we hypothesize that the fibrin gel film was thin enough to allow the embedded cells to sense the embedded PCL fibers with extended protrusions or that the cells were able to degrade the gel to get in contact with the aligned PCL fibers, which induced cell alignment through contact guidance. This modification could be used to prepare composite nanofiber/cell sheets that are ready for medical applications immediately after cell seeding. The processing time for fabricating both single- and multi-layered tissue engineering scaffolds is significantly lower for CN cell sheets compared to MF cell sheets. Several composite cell sheets may be stacked into a multilayered structure at one time, because layers are held together by external fixation while cell adhesions form. Procedures for fabricating multilayered structures from MF cell sheets may take 20 min to several hours per layer, since cell adhesions are required before the addition of the next layer [32,42,43].

While the CN cell sheet engineering approach offers great advantages associated with the biomaterial component (described above), it aims to minimize the amount of materials to be used to minimize the potential negative effects of the biomaterials, such as disturbance to cell-cell contacts and mass transport and activation of a foreign body response. According to our estimation, based upon fiber dimension, fiber density and the mass density of PCL, the total weight of the polymer required for a confluent composite nanofiber/cell sheet is in the tens of micrograms per cm². Because the nanofiber scaffolds have extremely low fiber densities, it is possible to achieve a porosity up to 75%, while maintaining a cell confluence greater than 90%. The composite cell sheets were robust, yet the increases in the weight and volume due to the presence of the nanofibers were very minimal. The ability of cells to move through the nanofiber sheets and populate on both sides further supports the hypothesis that cell-cell contacts experience minimal interference. Our choice of material in the specific form, *i.e.*, PCL nanofibers, have a long history of biomedical applications and are known for excellent biocompatibility. *In vitro* co-cultures of PCL nanofibers with many types of cells have not revealed any adverse effect of the material on any types of cells being examined [44–47]. PCL nanofibers elicited minimal tissue reactions in different types of tissues [48–50], and the extent of tissue reactions was related to the amount of implanted polymer and the form [51]. Although not examined in the present study, the composite cell sheets are not expected to elicit adverse tissue reactions at a local tissue site or systemically.

The excellent handling properties of these composite nanofiber/cell sheets have imparted their versatility in being processed into more complex, thick tissue structures of a higher hierarchy, including multilayered stacks and 3D self-assembled/bundled cable structures. These structures may be used as building blocks for clinically relevant implantable grafts. As shown in our data, individual layers of the sheets fused well with each other and were able to form a homogenous, aligned, tissue-like segment. Implantation studies for longer terms are underway to further assess the potential of the 3D constructs for aligned tissue engineering applications, such as wound healing, corneal, tendon, neural and skeletal and cardiac muscle regeneration. The varied geometries and compositions of these complex structures

expand their potential applications. The nanofiber component allows an additional degree of versatility, because biomolecules can be incorporated into polymer nanofibers. While biomolecule incorporation was not presented in this study, it is well established that many types of biomolecules can be attached to the surface of electrospun nanofibers or incorporated into them during fabrication for extended release [52]. To regenerate tissues of large dimensions, vascularization of the constructs is necessary. Hybrid cell sheets containing multiple cell types, including endothelial cells, may be used given appropriate guidance cues to promote vasculogenesis. Alternatively, endothelial cell sheets may be sandwiched among sheets of other cells before assembly into 3D structures. The simultaneous release of angiogenic growth factors locally at the implantation site may help to accelerate vascularization of the graft at a controlled vascular density. In addition, there are flexibilities in the material choices depending on the applications. For instance, materials of varying degradation profiles may be chosen for nanofiber fabrication to match the time course of regeneration in different types of tissues.

4. Conclusions

The recent development of a novel collecting method for electrospun fibers has made it possible to fabricate large-area, ultra-thin nanofiber sheets with well-controlled fiber orientation and density. It was found that aligned confluent cell sheets could form in culture in as few as three days on ultra-thin, extremely low density nanofiber sheets with porosities as high as 70%, and the overall polymer content was in the tens of micrograms per cm^2 of surface area. The aligned nanofiber sheets have guided the differentiation of myoblasts into aligned, linear myotubes on both sides of the sheets in spite of single-sided cell seeding. The nanofiber component of these scaffolds has significantly improved the mechanical properties, the handling and processing characteristics and the capacity for biomolecule storage/release. In addition, the overall amount of polymer nanofibers was reduced to minimize the interference with cell-cell contacts and mass transport. The handling properties of the composite cell sheets have allowed easy processing into 3D, more complex, thick structures of a higher hierarchy. Composite nanofiber/cell sheets retain the advantages of material-free cell sheets and traditional porous polymer scaffold-based sheets. Aligned ultrathin nanofiber array-based composite cell sheets hold promises in tissue engineering applications, such as wound healing, corneal, tendon, neural and skeletal and cardiac muscle regeneration.

Acknowledgments

This work was made possible by the NSF RII EPS-0903795 and the William H. Goodwin Endowment Funds.

Author Contributions

Vince Beachley, R. Glenn Hepfer and Eleni Katsanevakis did the experiments. Vince Beachley, Ning Zhang and Xuejun Wen analyzed the data and prepared the manuscript.

Conflicts of Interest

The authors declare no conflict of interest.

References

1. Hannachi, I.E.; Yamato, M.; Okano, T. Cell sheet technology and cell patterning for biofabrication. *Biofabrication* **2009**, *1*, doi:10.1088/1758-5082/1/2/022002.
2. Yang, J.; Yamato, M.; Kohno, C.; Nishimoto, A.; Sekine, H.; Fukai, F.; Okano, T. Cell sheet engineering: Recreating tissues without biodegradable scaffolds. *Biomaterials* **2005**, *26*, 6415–6422.
3. Sekiya, S.; Shimizu, T.; Yamato, M.; Kikuchi, A.; Okano, T. Bioengineered cardiac cell sheet grafts have intrinsic angiogenic potential. *Biochem. Biophys. Res. Commun.* **2006**, *341*, 573–582.
4. Shimizu, T.; Yamato, M.; Isoi, Y.; Akutsu, T.; Setomaru, T.; Abe, K.; Kikuchi, A.; Umezu, M.; Okano, T. Fabrication of pulsatile cardiac tissue grafts using a novel 3-dimensional cell sheet manipulation technique and temperature-responsive cell culture surfaces. *Circ. Res.* **2002**, *90*, e40–e48.
5. Nishida, K.; Yamato, M.; Hayashida, Y.; Watanabe, K.; Maeda, N.; Watanabe, H.; Yamamoto, K.; Nagai, S.; Kikuchi, A.; Tano, Y.; Okano, T. Functional bioengineered corneal epithelial sheet grafts from corneal stem cells expanded *ex vivo* on a temperature-responsive cell culture surface. *Transplantation* **2004**, *77*, 379–385.
6. Ohki, T.; Yamato, M.; Murakami, D.; Takagi, R.; Yang, J.; Namiki, H.; Okano, T.; Takasaki, K. Treatment of oesophageal ulcerations using endoscopic transplantation of tissue-engineered autologous oral mucosal epithelial cell sheets in a canine model. *Gut* **2006**, *55*, 1704–1710.
7. Watanabe, K.; Yamato, M.; Hayashida, Y.; Yang, J.; Kikuchi, A.; Okano, T.; Tano, Y.; Nishida, K. Development of transplantable genetically modified corneal epithelial cell sheets for gene therapy. *Biomaterials* **2007**, *28*, 745–749.
8. Canavan, H.E.; Cheng, X.; Graham, D.J.; Ratner, B.D.; Castner, D.G. Cell sheet detachment affects the extracellular matrix: A surface science study comparing thermal liftoff, enzymatic, and mechanical methods. *J. Biomed. Mater. Res. A* **2005**, *75*, 1–13.
9. Ide, T.; Nishida, K.; Yamato, M.; Sumide, T.; Utsumi, M.; Nozaki, T.; Kikuchi, A.; Okano, T.; Tano, Y. Structural characterization of bioengineered human corneal endothelial cell sheets fabricated on temperature-responsive culture dishes. *Biomaterials* **2006**, *27*, 607–614.
10. Da Silva, R.M.; Mano, J.F.; Reis, R.L. Smart thermoresponsive coatings and surfaces for tissue engineering: Switching cell-material boundaries. *Trends Biotechnol.* **2007**, *25*, 577–583.
11. Shimizu, T.; Yamato, M.; Kikuchi, A.; Okano, T. Two-dimensional manipulation of cardiac myocyte sheets utilizing temperature-responsive culture dishes augments the pulsatile amplitude. *Tissue Eng.* **2001**, *7*, 141–151.
12. Diehl, C.; Schlaad, H. Thermo-responsive polyoxazolines with widely tuneable LCST. *Macromol. Biosci.* **2009**, *9*, 157–161.
13. Ernst, O.; Lieske, A.; Jager, M.; Lankenau, A.; Duschl, C. Control of cell detachment in a microfluidic device using a thermo-responsive copolymer on a gold substrate. *Lab Chip* **2007**, *7*, 1322–1329.
14. Takezawa, T.; Mori, Y.; Yoshizato, K. Cell culture on a thermo-responsive polymer surface. *Nat. Biotechnology* **1990**, *8*, 854–856.
15. Tian, H.Y.; Yan, J.J.; Wang, D.; Gu, C.; You, Y.Z.; Chen, X.S. Synthesis of thermo-responsive polymers with both tunable UCST and LCST. *Macromol. Rapid Commun.* **2011**, *32*, 660–664.

16. Canavan, H.E.; Cheng, X.; Graham, D.J.; Ratner, B.D.; Castner, D.G. Surface characterization of the extracellular matrix remaining after cell detachment from a thermoresponsive polymer. *Langmuir* **2005**, *21*, 1949–1955.
17. Kim, Y.S.; Lim, J.Y.; Donahue, H.J.; Lowe, T.L. Thermoresponsive terpolymeric films applicable for osteoblastic cell growth and noninvasive cell sheet harvesting. *Tissue Eng.* **2005**, *11*, 30–40.
18. Kwon, O.H.; Kikuchi, A.; Yamato, M.; Sakurai, Y.; Okano, T. Rapid cell sheet detachment from poly(N-isopropylacrylamide)-grafted porous cell culture membranes. *J. Biomed. Mater. Res.* **2000**, *50*, 82–89.
19. Asran, A.; Razghandi, K.; Aggarwal, N.; Michler, G.H.; Groth, T. Nanofibers from blends of polyvinyl alcohol and polyhydroxy butyrate as potential scaffold material for tissue engineering of skin. *Biomacromolecules* **2010**, *11*, 3413–3421.
20. Fang, R.; Zhang, E.; Xu, L.; Wei, S. Electrospun PCL/PLA/HA based nanofibers as scaffold for osteoblast-like cells. *J. Nanosci. Nanotechnol.* **2010**, *10*, 7747–7751.
21. Tambralli, A.; Blakeney, B.; Anderson, J.; Kushwaha, M.; Andukuri, A.; Dean, D.; Jun, H.W. A hybrid biomimetic scaffold composed of electrospun polycaprolactone nanofibers and self-assembled peptide amphiphile nanofibers. *Biofabrication* **2009**, *1*, doi:10.1088/1758-5082/1/2/025001.
22. Huang, L.; Nagapudi, K.; Apkarian, R.P.; Chaikof, E.L. Engineered collagen-PEO nanofibers and fabrics. *J. Biomater. Sci. Polym. Ed.* **2001**, *12*, 979–993.
23. Beachley, V.; Katsanevakis, E.; Zhang, N.; Wen, X. A novel method to precisely assemble loose nanofiber structures for regenerative medicine applications. *Adv. Healthc. Mater.* **2013**, *2*, 343–351.
24. Beachley, V.; Wen, X. Fabrication of Three Dimensional Aligned Nanofiber Array. U.S. Patent 7,828,539, 2010.
25. Beachley, V.; Wen, X.J. Fabrication of nanofiber reinforced protein structures for tissue engineering. *Mater. Sci. Eng. C Mater. Biol. Appl.* **2009**, *29*, 2448–2453.
26. Boudaoud, A.; Burian, A.; Borowska-Wykret, D.; Uyttewaal, M.; Wrzalik, R.; Kwiatkowska, D.; Hamant, O. Fibriltool, an imagej plug-in to quantify fibrillar structures in raw microscopy images. *Nat. Protoc.* **2014**, *9*, 457–463.
27. Choi, J.S.; Lee, S.J.; Christ, G.J.; Atala, A.; Yoo, J.J. The influence of electrospun aligned poly(epsilon-caprolactone)/collagen nanofiber meshes on the formation of self-aligned skeletal muscle myotubes. *Biomaterials* **2008**, *29*, 2899–2906.
28. Mathur, A.B.; Collinsworth, A.M.; Reichert, W.M.; Kraus, W.E.; Truskey, G.A. Endothelial, cardiac muscle and skeletal muscle exhibit different viscous and elastic properties as determined by atomic force microscopy. *J. Biomech.* **2001**, *34*, 1545–1553.
29. Shiroyanagi, Y.; Yamato, M.; Yamazaki, Y.; Toma, H.; Okano, T. Urothelium regeneration using viable cultured urothelial cell sheets grafted on demucosalized gastric flaps. *BJU Int.* **2004**, *93*, 1069–1075.
30. Hasegawa, M.; Yamato, M.; Kikuchi, A.; Okano, T.; Ishikawa, I. Human periodontal ligament cell sheets can regenerate periodontal ligament tissue in an athymic rat model. *Tissue Eng.* **2005**, *11*, 469–478.

31. L'Heureux, N.; Dusserre, N.; Konig, G.; Victor, B.; Keire, P.; Wight, T.N.; Chronos, N.A.F.; Kyles, A.E.; Gregory, C.R.; Hoyt, G.; Robbins, R.C.; McAllister, T.N. Human tissue-engineered blood vessels for adult arterial revascularization. *Nat. Med.* **2006**, *12*, 361–365.
32. Takahashi, H.; Shimizu, T.; Nakayama, M.; Yamato, M.; Okano, T. The use of anisotropic cell sheets to control orientation during the self-organization of 3D muscle tissue. *Biomaterials* **2013**, *34*, 7372–7380.
33. Dang, J.M.; Leong, K.W. Myogenic induction of aligned mesenchymal stem cell sheets by culture on thermally responsive electrospun nanofibers. *Adv. Mater. Deerfield* **2007**, *19*, 2775–2779.
34. Birch, M.A.; Tanaka, M.; Kirmizidis, G.; Yamamoto, S.; Shimomura, M. Microporous “honeycomb” films support enhanced bone formation *in vitro*. *Tissue Eng. A* **2013**, *19*, 2087–2096.
35. Kikuchi, A.; Okano, T. Nanostructured designs of biomedical materials: Applications of cell sheet engineering to functional regenerative tissues and organs. *J. Control Release* **2005**, *101*, 69–84.
36. Yamato, M.; Konno, C.; Utsumi, M.; Kikuchi, A.; Okano, T. Thermally responsive polymer-grafted surfaces facilitate patterned cell seeding and co-culture. *Biomaterials* **2002**, *23*, 561–567.
37. Yamato, M.; Kwon, O.H.; Hirose, M.; Kikuchi, A.; Okano, T. Novel patterned cell coculture utilizing thermally responsive grafted polymer surfaces. *J. Biomed. Mater. Res.* **2001**, *55*, 137–140.
38. Hirose, M.; Kwon, O.H.; Yamato, M.; Kikuchi, A.; Okano, T. Creation of designed shape cell sheets that are noninvasively harvested and moved onto another surface. *Biomacromolecules* **2000**, *1*, 377–381.
39. Konig, G.; McAllister, T.N.; Dusserre, N.; Garrido, S.A.; Iyican, C.; Marini, A.; Fiorillo, A.; Avila, H.; Wystrychowski, W.; Zagalski, K.; Maruszewski, M.; Jones, A.L.; Cierpka, L.; de la Fuente, L.M.; L'Heureux, N. Mechanical properties of completely autologous human tissue engineered blood vessels compared to human saphenous vein and mammary artery. *Biomaterials* **2009**, *30*, 1542–1550.
40. Isenberg, B.C.; Backman, D.E.; Kinahan, M.E.; Jesudason, R.; Suki, B.; Stone, P.J.; Davis, E.C.; Wong, J.Y. Micropatterned cell sheets with defined cell and extracellular matrix orientation exhibit anisotropic mechanical properties. *J. Biomech.* **2012**, *45*, 756–761.
41. Takahashi, H.; Nakayama, M.; Shimizu, T.; Yamato, M.; Okano, T. Anisotropic cell sheets for constructing three-dimensional tissue with well-organized cell orientation. *Biomaterials* **2011**, *32*, 8830–8838.
42. Matsusaki, M.; Kadowaki, K.; Nakahara, Y.; Akashi, M. Fabrication of cellular multilayers with nanometer-sized extracellular matrix films. *Angew. Chem. Int. Ed.* **2007**, *46*, 4689–4692.
43. Tsuda, Y.; Shimizu, T.; Yamato, M.; Kikuchi, A.; Sasagawa, T.; Sekiya, S.; Kobayashi, J.; Chen, G.; Okano, T. Cellular control of tissue architectures using a three-dimensional tissue fabrication technique. *Biomaterials* **2007**, *28*, 4939–4946.
44. Reed, C.R.; Han, L.; Andrady, A.; Caballero, M.; Jack, M.C.; Collins, J.B.; Saba, S.C.; Lobo, E.G.; Cairns, B.A.; van Aalst, J.A. Composite tissue engineering on polycaprolactone nanofiber scaffolds. *Ann. Plast. Surg.* **2009**, *62*, 505–512.
45. Hashemi, S.M.; Soleimani, M.; Zargarian, S.S.; Haddadi-Asl, V.; Ahmadbeigi, N.; Soudi, S.; Gheisari, Y.; Hajarizadeh, A.; Mohammadi, Y. *In vitro* differentiation of human cord blood-derived unrestricted somatic stem cells into hepatocyte-like cells on poly(epsilon-caprolactone) nanofiber scaffolds. *Cells Tissues Organs* **2009**, *190*, 135–149.

46. Subramanian, A.; Krishnan, U.M.; Sethuraman, S. Fabrication, characterization and *in vitro* evaluation of aligned PLGA-PCL nanofibers for neural regeneration. *Ann. Biomed. Eng.* **2012**, *40*, 2098–2110.
47. Gumusderelioglu, M.; Dalkiranoglu, S.; Aydin, R.S.; Cakmak, S. A novel dermal substitute based on biofunctionalized electrospun PCL nanofibrous matrix. *J. Biomed. Mater. Res. A* **2011**, *98*, 461–472.
48. Hoppen, H.J.; Leenslag, J.W.; Pennings, A.J.; van der Lei, B.; Robinson, P.H. Two-ply biodegradable nerve guide: Basic aspects of design, construction and biological performance. *Biomaterials* **1990**, *11*, 286–290.
49. Den Dunnen, W.F.; van der Lei, B.; Robinson, P.H.; Holwerda, A.; Pennings, A.J.; Schakenraad, J.M. Biological performance of a degradable poly(lactic acid-epsilon-caprolactone) nerve guide: Influence of tube dimensions. *J. Biomed. Mater. Res.* **1995**, *29*, 757–766.
50. Den Dunnen, W.F.; van der Lei, B.; Schakenraad, J.M.; Blaauw, E.H.; Stokroos, I.; Pennings, A.J.; Robinson, P.H. Long-term evaluation of nerve regeneration in a biodegradable nerve guide. *Microsurgery* **1993**, *14*, 508–515.
51. Ekholm, M.; Hietanen, J.; Lindqvist, C.; Rautavuori, J.; Santavirta, S.; Suuronen, R. Histological study of tissue reactions to epsilon-caprolactone-lactide copolymer in paste form. *Biomaterials* **1999**, *20*, 1257–1262.
52. Beachley, V.; Wen, X. Polymer nanofibrous structures: Fabrication, biofunctionalization, and cell interactions. *Prog. Polym. Sci.* **2010**, *35*, 868–892.

© 2014 by the authors; licensee MDPI, Basel, Switzerland. This article is an open access article distributed under the terms and conditions of the Creative Commons Attribution license (<http://creativecommons.org/licenses/by/3.0/>).